

Ultrastretchable MXene Microsupercapacitors

Menglu Wang, Shuxuan Feng, Chong Bai, Kang Ji, Jiaxue Zhang, Shaolei Wang, Yanqing Lu,* and Desheng Kong*

Stretchable microsupercapacitors represent emerging miniaturized energy-storage devices for next-generation deformable electronics. Two-dimensional (2D) transition metal carbides (MXenes) are considered attractive electrode materials due to their metallic conductivity, hydrophilic surfaces, and excellent processability. Here, an ultrastretchable microsupercapacitor of interdigitated MXene microelectrodes with crumpled surface textures is created. The microsupercapacitor shows a series of attractive properties including a high specific capacitance of $\approx 185 \text{ mF cm}^{-2}$, ultrahigh stretchability up to 800% area strain, and $\approx 89.7\%$ retention of the initial capacitance after 1000 stretch–relaxation cycles. In addition to static strains, the microsupercapacitor demonstrates robust mechanical properties to retain stable charging–discharging capability under dynamic stretching at different strain rates. A self-powering circuit system utilizes four microsupercapacitor packs to power a light-emitting diode (LED) array, which exhibits stable operations under large tensile strain and skin-attached wearable settings. The developments offer a generic design strategy to enhance the deformability of microsupercapacitors based on 2D nanomaterials.

Compatible energy storage and conversion devices are urgently required for an untethered self-powering system, including batteries, supercapacitors, solar cells, and nanogenerators.^[13–19] To this end, stretchable microsupercapacitors represent attractive candidates in terms of their compact design, planar structure, and facile system integrations.^[20–22] In addition, the output voltage and total capacitance are easily adjustable by connecting microsupercapacitor in series, parallel, and parallel-series, in order to match the demands of corresponding electronic circuits.^[23–25] The stretchable forms of microsupercapacitors are therefore considered the key enabling energy storage device for next-generation wearable electronic gadgets.

Several approaches are currently available to create stretchable microsupercapacitors. Conventional rigid devices in matrix forms have been interconnected

with compliant conductors on elastomer substrates. The tensile loadings are primarily accommodated by the elongation of compliant conductors to achieve mechanical deformability on the system level.^[21,26,27] The discrete matrix design unfortunately reduces the device area and hence the specific capacitance. An alternative strategy utilizes microstructured electrodes with rich internal space to enable large tensile deformations, including crumpled surface wrinkles and serpentine-like patterns.^[28–32] Apart from the delicate structural designs, the active material loading is often carefully controlled to avoid structural failures upon stretching due to the inherently high stiffness. The corresponding microsupercapacitors often show a significant trade-off between electrochemical performances and mechanical deformability. Intrinsically stretchable microsupercapacitor harness all compliant electrodes to achieve skin-like mechanical properties.^[20,33,34] In spite of the facile fabrication procedures, the rapidly increased electrode resistance upon stretching, unfortunately, limits the practical deformability of these devices.

MXenes are a rising family of 2D materials featuring metallic conductivity, hydrophilic surfaces, and excellent processability.^[35,36] MXenes are widely recognized as attractive electrode materials of supercapacitors with combined double-layer and redox-type ion storage mechanisms.^[37–39] Colloid MXene nanosheets are delaminated from bulk crystals and then reassembled into flexible composite films.^[40,41] A transfer printing technique conveniently generates crumpled MXene electrodes


1. Introduction

Stretchable electronics represent a disruptive technology feature compliant mechanical properties and facile integration with the human body.^[1–4] The conformal and seamless interface with the skin is established by stretchable electronics for cutting-edge applications in advanced health monitoring,^[5–7] wearable therapy,^[8,9] and smart human-machine interfaces.^[10–12]

M. Wang, S. Feng, C. Bai, K. Ji, J. Zhang, S. Wang, Y. Lu, D. Kong
College of Engineering and Applied Sciences
National Laboratory of Solid State Microstructures
and Collaborative Innovation Center of Advanced Microstructures
Nanjing University
Nanjing 210093, P. R. China
E-mail: yqlu@nju.edu.cn; dskong@nju.edu.cn

Y. Lu
Key Laboratory of Intelligent Optical Sensing and Manipulation
Nanjing University
Nanjing 210093, P. R. China

D. Kong
State Key Laboratory of Analytical Chemistry for Life Science
and Jiangsu Key Laboratory of Artificial Functional Materials
Nanjing University
Nanjing 210046, P. R. China

 The ORCID identification number(s) for the author(s) of this article can be found under <https://doi.org/10.1002/sml.202300386>.

DOI: 10.1002/sml.202300386

on elastomer substrates.^[32,42,43] Due to the exceptional mechanical flexibility of MXene films, the wrinkled surfaces of fairly-thick MXene electrodes can still retain reliable electrical conductivity and electrochemical performances under large tensile deformations.^[42] The attractive properties of crumpled MXene electrodes have rarely been exploited to create stretchable microsupercapacitor. In the context of microsupercapacitor applications, stretchable MXene electrodes have already been achieved with porous honeycomb scaffold designs.^[20] Despite excellent electrochemical performances, the corresponding microsupercapacitor exhibits limited stretchability within 50% uniaxial tensile strain.

In this study, we report the design and fabrication of an ultrastretchable MXene microsupercapacitor featuring high specific area capacitance and exceptional mechanical deformability. A crumpled electrode is prepared by transferring MXene/Au composite film onto prestretched substrate, followed by laser patterning into the interdigitated structure. The deposited Au layer serves as the current collector to boost the rate capability. The MXene microsupercapacitor has a specific capacitance of 185 mF cm^{-2} at 2.0 mV s^{-1} and excellent electrochemical cycling stability. The crumpled surface of the MXene electrode is the enabler of mechanical deformability to accommodate biaxial tensions up to 800% area strain. In addition to static strains, the microsupercapacitor maintains stable charging–discharging capability under dynamic tensile loadings commonly encountered in practical applications. As prepared microsupercapacitor cells are easily combined by compliant interconnects to adjust the total outputs. A self-powering circuit system containing a LED array and four microsupercapacitor cells is successfully assembled to achieve reliable operation under biaxial deformations to 800% area strain. The MXene microsupercapacitor exhibits attractive electrochemical performances and

ultrahigh mechanical stretchability, which represents promising energy storage devices for emerging applications in skin-attachable sensors, smart wearables, and soft robotics.

2. Results and Discussion

The fabrication process flow of stretchable MXene microelectrodes is schematically illustrated in **Figure 1a**. Briefly, a $\text{Ti}_3\text{C}_2\text{T}_x$ MXene film is created from the aqueous colloid dispersion by vacuum-assisted filtration. Here, $\text{Ti}_3\text{C}_2\text{T}_x$ MXene nanosheets are top-down synthesized from Ti_3AlC_2 MAX phase powders, as confirmed by structural characterizations in Figure S1, Supporting Information. A 100 nm-thick Au film is subsequently deposited onto the MXene film by thermal evaporation to serve as the current collector.^[44,45] The composite film is manually transferred onto a biaxially prestrained substrate of acrylic elastomer from the filter membrane. A stretchable electrode is formed through a buckle-delamination process to convert MXene film into microwrinkled morphology by releasing the tensile strain (see Figure S2, Supporting Information).^[46] Selective laser ablation is employed for the maskless patterning of the MXene electrode into an interdigitated structure.^[47,48] The acrylic elastomer is highly transparent at near infrared wavelengths (Figure S3, Supporting Information). The strong absorptions of the MXene film to near-infrared lights lead to efficient heat conversion upon laser irradiations (see Figure S3, Supporting Information). The significant contrast in optical properties ensures the selective patterning of MXene films without collateral damage to the substrate. A representative optical image of MXene microelectrode is shown in Figure 1b. The microelectrode is mechanically deformable to allow biaxial stretching to 800% area strain. In Figure 1c, the microscopy

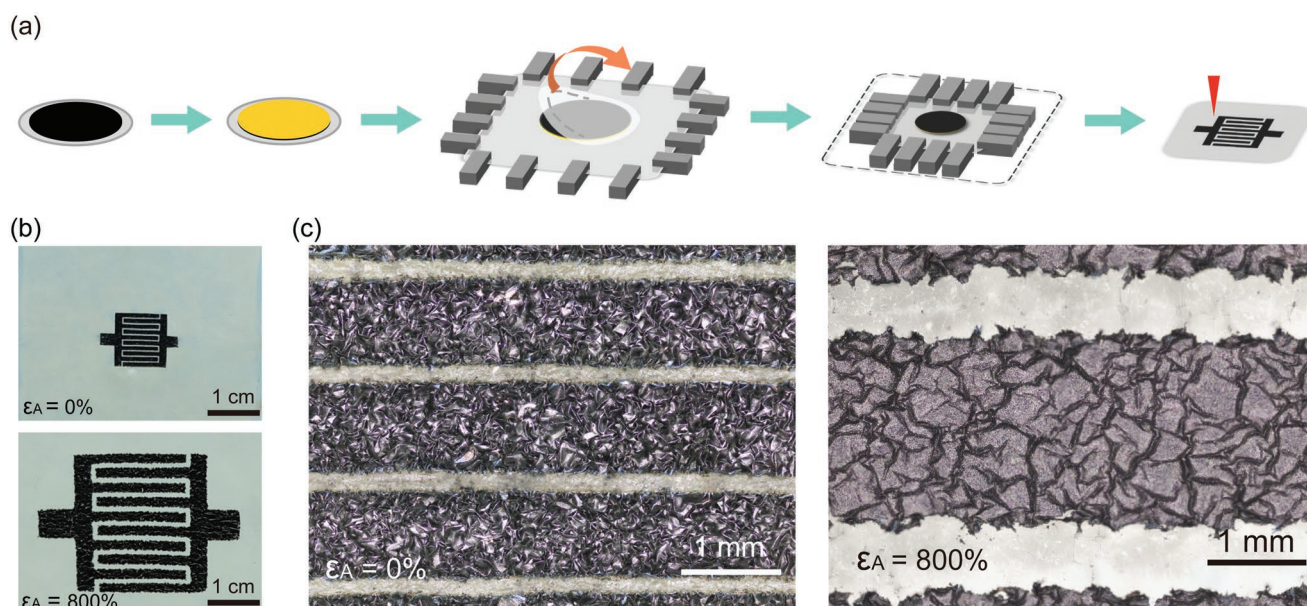


Figure 1. Fabrication and characterization of ultrastretchable MXene microsupercapacitor. a) Schematic illustration of the process flow to create a stretchable MXene-based microsupercapacitor. b) Optical images of the microsupercapacitors at the relaxed state (top) and biaxially stretched state with 800% area strain (bottom). c) Corresponding optical microscopy images to reveal the microstructure of the electrodes at 0% (left) and 800% (right) strains.

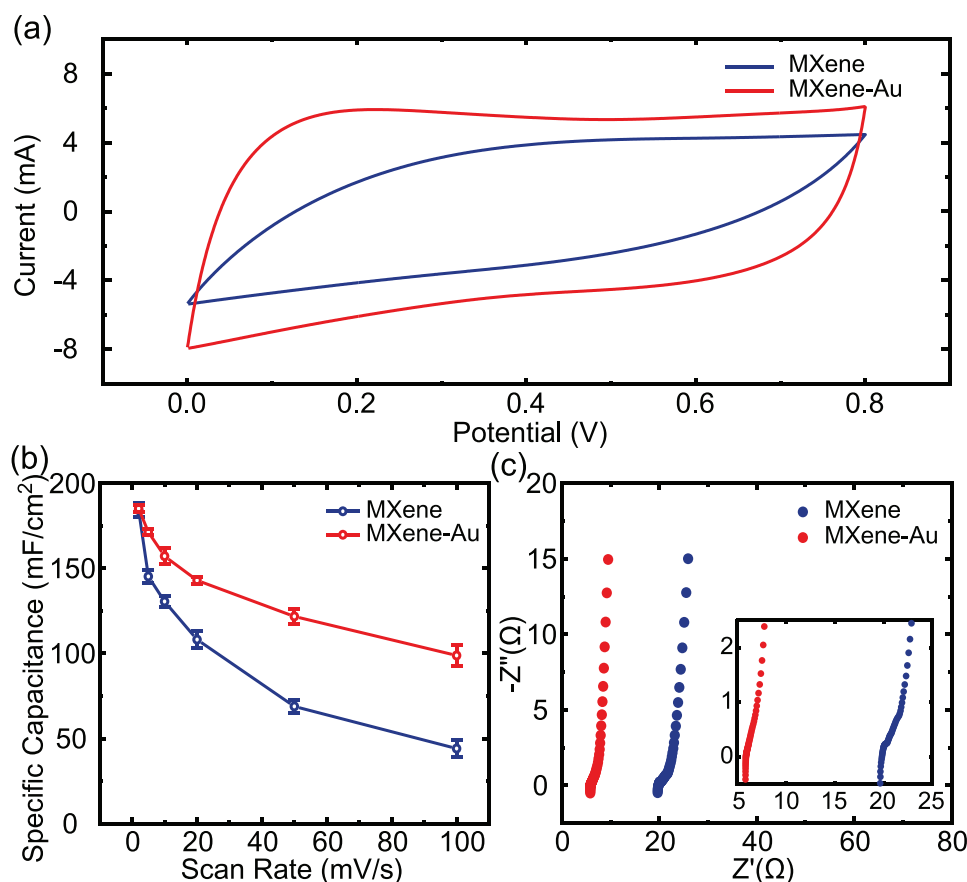


Figure 2. a) CV curves of MXene and MXene-Au composite microsupercapacitors at a scan rate of 50 mV s^{-1} . b) Specific area capacitance as a function of scan rate based on CV curves. c) Nyquist plots from EIS spectra of microsupercapacitors at the fully relaxed states. The inset shows the magnified Nyquist plots at high-frequency regions.

image reveals the crumpled morphology of individual microelectrode and the geometric dimension of the interdigitated structure ($850/250 \text{ } \mu\text{m}$, electrode/gap). The individual microelectrode is capable of accommodating ultrahigh tensile deformations by unfolding the microwrinkles. Here, the MXene film represents indispensable mechanical support to retain the structural integrity of the wrinkled composite electrode.^[49,50] In contrast, the crumpled Au electrode is largely cracked upon stretching due to the extremely low fracture strain of free-standing film (see Figure S2, Supporting Information).^[51]

In terms of the device assembly, the interdigitated microelectrodes are covered with PVA- H_3PO_4 gel electrolyte and then encapsulated with an acrylic elastomer film. Figure 2a shows cyclic voltammetry (CV) curves of the as-prepared microsupercapacitor at a scan rate of 50 mV s^{-1} . The quasi-rectangular shaped curve is obtained from the composite MXene/Au microelectrode to suggest excellent capacitive behavior.^[52,53] In contrast, the CV curve of the MXene microelectrode at the same scan rate is inclined remarkably. In Figure 2b, the specific capacitance values at different scan rates are determined based on the CV curves. A high area capacitance of $\approx 185 \text{ mF cm}^{-2}$ is achieved at 2.0 mV s^{-1} for both types of electrodes. The composite microelectrode has higher capacitance by increasing the scan rate. In Figure 2c, electrochemical impedance spectroscopy

(EIS) analysis reveals reduced cell resistance of the composite electrode by introducing Au film as the current collector. The microsupercapacitor based on the composite MXene/Au microelectrode, therefore, achieves excellent rate capability.

We further explore the influence of MXene film thickness on the transferred electrodes. According to scanning electron microscopy (SEM) images in Figure 3a, the dimension of the surface wrinkles expands by increasing the thickness and hence the stiffness of MXene film. The electromechanical stability of the crumpled MXene electrode is measured through biaxially strain-controlled fatigue tests involving 1000 stretch-relaxation cycles to 800% area strain. The liquid metal-based deformable contacts are printed onto the MXene electrode to enable four-probe resistance measurements under different tensile strains, as illustrated in Figure 3b. In Figure 3c, the normalized resistance (R/R_0) shows negligible changes upon stretching for MXene films ranging from 2.2 to $3.2 \text{ } \mu\text{m}$. The stable electrical properties are consistent with the intact morphology of the electrodes (see Figure S4, Supporting Information). In contrast, the rapidly increased resistance in $3.9 \text{ } \mu\text{m}$ -thick MXene film is associated with the emergence of cracks that disrupt the structural integrity, as shown in Figure S4, Supporting Information. The thick film with high bending stiffness tends to fracture during repetitive stress conditions.^[46,54] In addition, the electrochemical

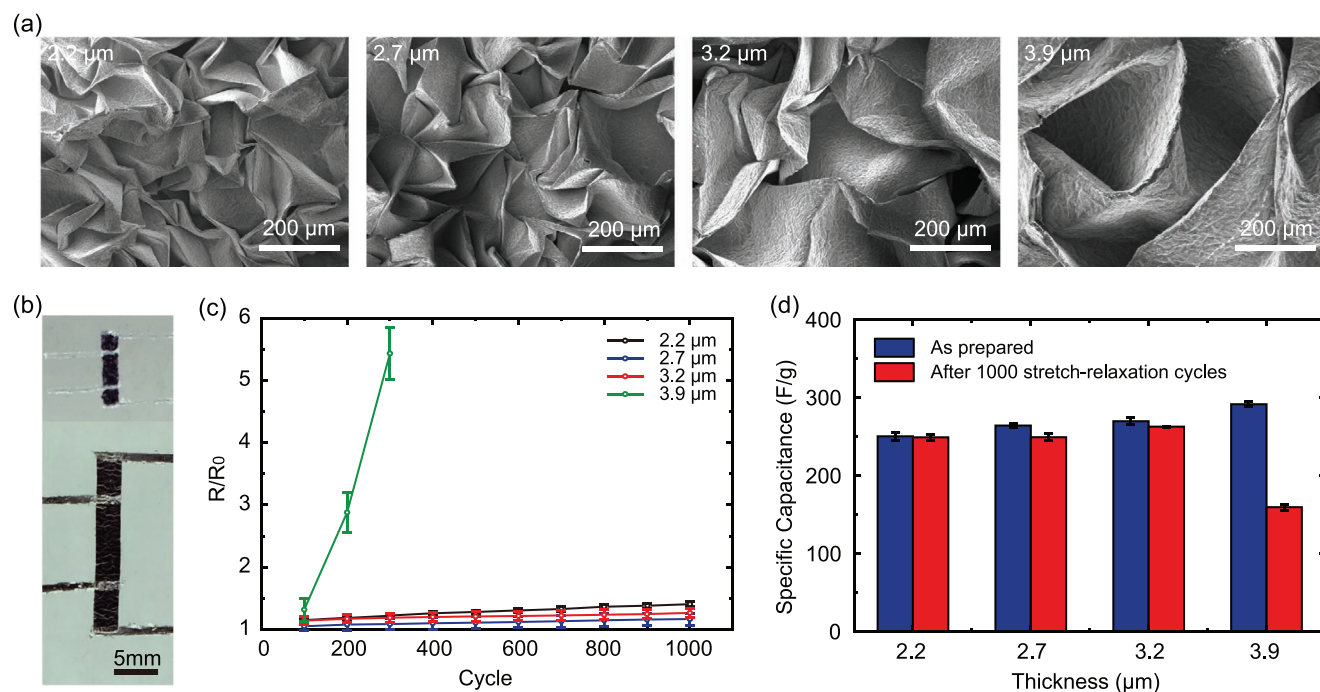


Figure 3. Influence of MXene film thickness on electromechanical and electrochemical properties of the microsupercapacitor. a) SEM images of crumpled electrodes based on MXene films of different thicknesses. b) Optical images of stretchable MXene electrode for the four-probe resistance measurement at 0% (top) and 800% area strains (bottom). c) Evolution of the normalized resistance over 1000 stretch–relaxation cycles to 800% area strain. d) Specific gravimetric capacitance at the pristine state and after 1000 stretch cycles.

performance is another critical aspect of the electrode design. As shown in Figure 3d, the specific gravimetric capacitance of thin electrodes is well retained during 1000 stretch–relaxation cycles to 800% strain. The notably reduced capacitance is encountered in 3.9 μm-thick MXene film due to substantial structural damages. Accordingly, ≈3.2 μm-thick MXene film represents the optimal choice by combining excellent mechanical durability and high area capacitance.

In Figure 4a, CV curves of the microsupercapacitor exhibit a rectangular shape at different scan rates from 2.0 to 100 mV s^{−1}. The capacitive storage behavior is further supported by the triangular shaped galvanostatic charge/discharge (GCD) curves at a current density of 1.0 A g^{−1}, as shown in Figure S5, Supporting Information. The electrochemical stability is confirmed by the stable GCD curves and the high capacitance retention of 84.9% after 10000 GCD cycles, as shown in Figure 4b. The microsupercapacitor exhibits compliant mechanical properties to accommodate large tensile deformations. In Figure 4c, CV curves at 20 mV s^{−1} of the microsupercapacitor are fairly stable under large biaxial tensile deformations. The capacitance retention is 84.4% at 800% area strain (see Figure 4d). The minor decrease in capacitance is ascribed to the increased cell resistance with the expanded interdigitated gaps, according to EIS analysis in Figure S6, Supporting Information. Compared with reported MXene microsupercapacitors, our device demonstrates a competitive area capacitance and order-of-magnitude improved stretchability, as shown in Figure S7, Supporting Information.^[20,52,55–61] The superior performance is associated with the crumpled electrode design to accommodate the enormous strains. In addition, the microsupercapacitor demon-

strates high capacitance retention of 89.7% after 1000 stretch–relaxation cycles to 800% strain, as shown in Figure 4e. The exceptional durability in the fatigue test is associated with the robust mechanical properties of the MXene electrode. In addition to the static strains, the dynamic strain loadings on the microsupercapacitor are commonly encountered in practical application settings.^[31,42] In Figure 4f, GCD profile is acquired during the stretch–relaxation cycles to 800% area strain at different strain rates, which essentially overlaps with the profile at the relaxed state. The stable electrochemical performances demonstrate robust mechanical properties to withstand unexpected loadings and sudden impacts. Apart from area strains, the microsupercapacitor can also survive uniaxial tensile deformations as shown in Figure S8, Supporting Information. The capacitance is retained at 89.0% of the initial value under a uniaxial strain of 200%.

The planar configuration of the microsupercapacitor allows the facile interconnection of multiple cells to modulate output voltages and total capacitance, as schematically demonstrated in the equivalent circuit diagrams in Figure 5a. GCD profiles of serially connected microsupercapacitor exhibit linearly increased voltage from 0.8 to 3.2 V and similar charging/discharging time (see Figure 5b). In spite of the same voltage window, the parallel connected microsupercapacitors demonstrate extended discharge time in proportion to the cell numbers (Figure 5c). In addition, CV curves of interconnected supercapacitors essentially yield consistent results, as shown in Figure S9, Supporting Information. The soft pack comprising multiple integrated cells effectively boosts the output characteristics to match the corresponding stretch-

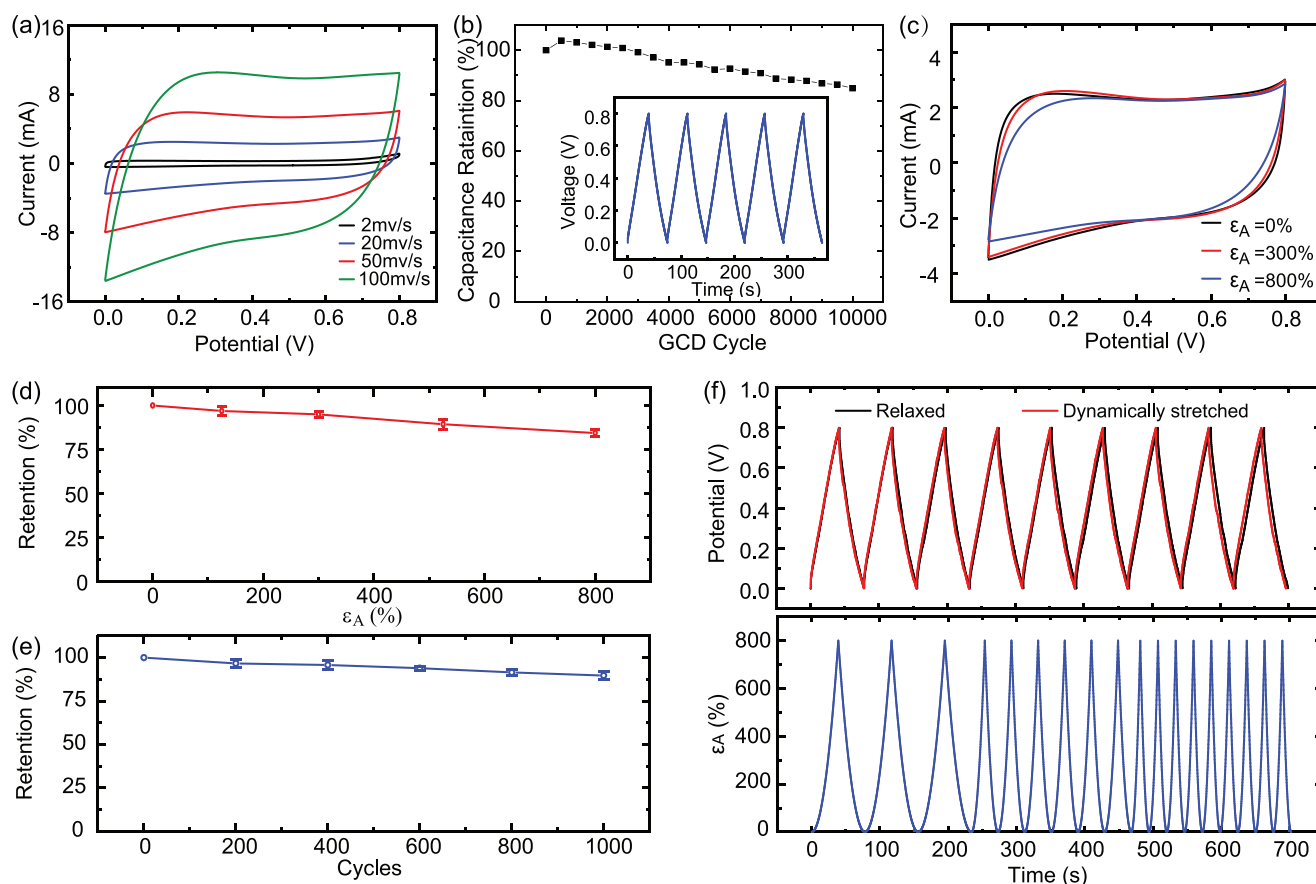


Figure 4. Electrochemical performance of the microsupercapacitor under relaxed and stretched conditions. a) CV curves acquired at different scan rates from 2.0 to 100 mV s^{-1} . b) Capacitance retention during GCD cycles at a current density of 1.0 A g^{-1} . Inset: The corresponding GCD curve. c) CV curves at 20 mV s^{-1} acquired from a stretchable microsupercapacitor under different area strains. d) Capacitance retention for biaxially tensile deformations. e) Capacitance retention for stretch–relaxation cycles to 800% strain. f) GCD curves of stretchable microsupercapacitor under relaxed and dynamically stretched conditions. Corresponding area strain as a function of time for dynamic stretching processes at varying strain rates of 20, 40, and 60 s^{-1} .

able electronic devices. According to the schematic illustration in Figure 5d, four microsupercapacitor cells are assembled in series to power a stretchable LED array. The maximum charging voltage of 3.2 V of the integrated cell pack is sufficient for the LED to achieve bright emissions, thereby establishing a self-powering electronic system. The deformable characteristic of the electronic system allows stable operations under large tensile deformations up to 800% strain (see Figure 5e and Video S1, Supporting Information). The self-powering system is conformally attached to the wrist as an epidermal light source, which retains reliable emission irrespective of hand motions (see Figure 5f and Video S2, Supporting Information).

3. Conclusion

In summary, we have established the material design and scalable fabrication of an ultrastretchable MXene microsupercapacitor. The crumpled morphology of the MXene/Au composite electrode provides sufficient internal space to accommodate large tensile deformations. The as-prepared microsupercapacitor shows a high specific capacitance of $\approx 185 \text{ mF cm}^{-2}$, excel-

lent electrochemical stability, and ultrahigh stretchability up to 800% area strain. The device retains stable electrochemical performances under both static and dynamic tensile deformations. The output voltage and capacitance are easily adjusted by interconnecting multiple cells in series or parallel. An integrated self-powering electronic system harnesses four microsupercapacitor cells to drive an LED array and achieves reliable operation at 800% area strain. A promising design strategy is established here to create ultrastretchable MXene microsupercapacitors, which may generally be applicable to other 2D nanomaterials.

4. Experimental Section

Material Experimental Methods: All raw materials and chemical reagents were purchased from corresponding vendors, including Ti_3AlC_2 powder from TI Technology Co., Ltd., gold pellets from Yipin Chuancheng Technology Co., Ltd., LiF (99.99%) from Shanghai Energy Chemicals Co., Ltd., HCl and H_3PO_4 from Shanghai Macklin Biochemical Co., Ltd., and PVA ($M_w = 205 \text{ K}$) from Sigma Aldrich, Inc. The acrylic elastomer substrates (VHB 4905, VHB 4910) were obtained from 3 M Inc. The

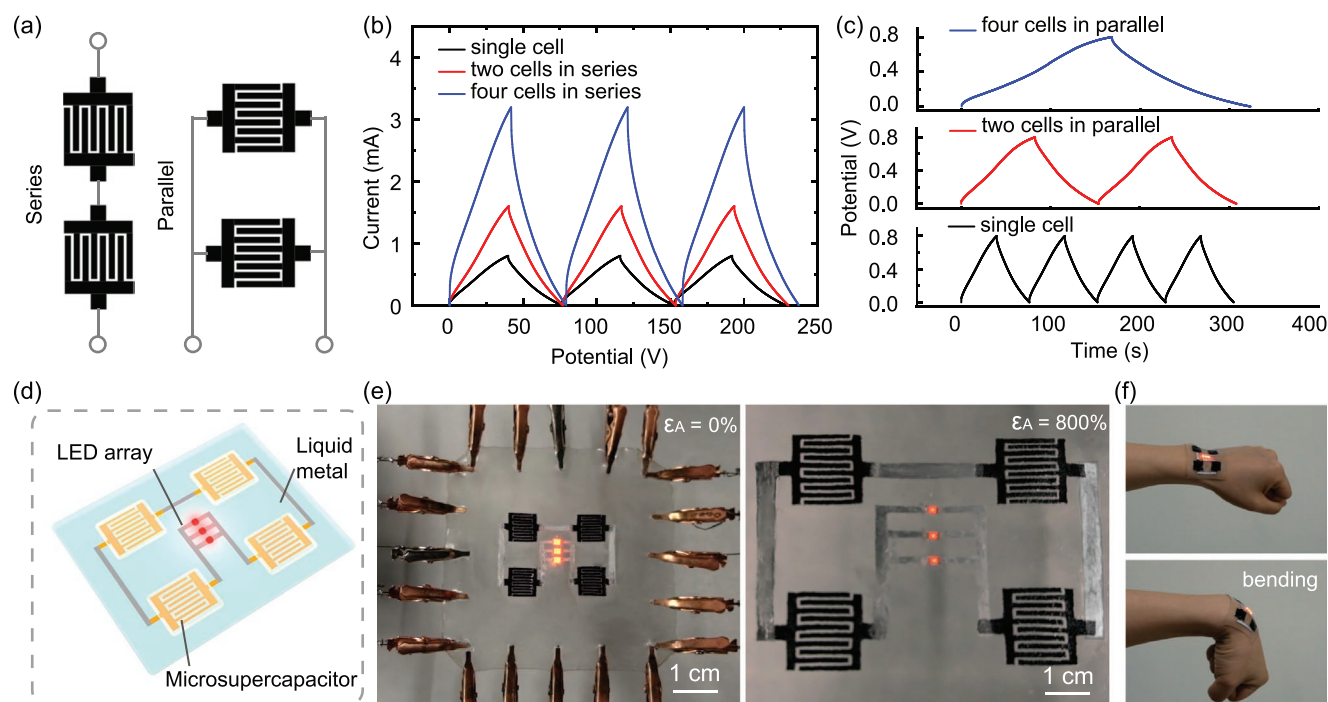


Figure 5. Integration of stretchable microsupercapacitors for self-powering wearable electronic systems. a) Schematic diagram of four microsupercapacitors connected in series and parallel. GCD curves at 1.0 A g^{-1} of the multiple microsupercapacitors connected b) in series and c) in parallel. d) Schematic illustration of the self-powering wearable electronic system. e) Optical images of a self-powering electronic system at 0% (left) and 800% (right) area strains. f) Optical images of the system with conformal attachment to the human wrist.

liquid metal was prepared by melting a mixture of metal pieces of Ga, In, and Sn with a weight ratio of 68.5: 21.5:10 at 80°C for 2 h in a glovebox. In order to formulate a screen printable ink, as-prepared liquid metal was partially oxidized into a viscous slurry by stirring at 200 rpm for 10 min under ambient conditions. A modified version of the minimally intensive layer delamination (MILD) method was adopted to produce $\text{Ti}_3\text{C}_2\text{T}_x$ MXene aqueous dispersion (2.0 mg mL^{-1}) from Ti_3AlC_2 powder.

Preparation of Stretchable Microsupercapacitor: The MXene film was prepared by vacuum-assisted filtration of a PVDF membrane ($0.22 \mu\text{m}$, $\Phi = 5 \text{ cm}$), followed by drying in a vacuum oven at 50°C for 2 h. The thickness of the MXene film was controlled by adjusting the volume of the colloid dispersion. A 100 nm-thick Au layer was subsequently deposited onto MXene film in a ZHD400 thermal evaporator from Beijing Technol Science Co., Ltd. A 1 mm-thick acrylic elastomer substrate was first biaxially stretched to reach an area strain of 800% on the motorized translational linear stage. The filter membrane was gently pressed against the deformed substrate. After peeling off the membrane, the MXene film was transferred onto the elastomer substrate. The crumpled morphology was formed by releasing the strain. The interdigitated electrodes were subtractively patterned by selective laser ablation using a 1064 nm benchtop laser marking system (XM-FB30, Xianming Optoelectronic Equipment Co., Ltd). The gel electrolyte was prepared by dissolving 3 g PVA into 30 mL of 5 M H_3PO_4 . Then the PVA- H_3PO_4 gel electrolyte was drop-cast onto the whole interdigitated supercapacitor. The VHB tape was used to encapsulate microsupercapacitor to form a water-tight seal from the electrolyte. Multiple prepared microsupercapacitors were connected in series or in parallel through liquid metal to carry out CV and GCD tests.

Fabrication of the Stretchable Electronic Device: The stretchable electronic device is composed of four MXene microsupercapacitors and a deformable LED array. Power was supplied by four serially microsupercapacitors. The four films were transferred to a specific location onto the same VHB substrate of 800% biaxial pre-stretched. Releasing the strain and cutting into the interdigital electrode pattern by using a 1064 nm laser marking system. The liquid metal circuit

pattern was printed with a paper stencil by laser cutting. LED chips were mounted onto contact pads in the circuit pattern by the adhesive property of the VHB tape. The electrolyte was evenly covered on each pair of electrodes, and then the stretchable electronic device was encapsulated by covering VHB tape.

Materials Characterizations: Optical images and video were acquired by a Fujifilm X-T10 camera. Structural and compositional characterizations involved SEM using a Zeiss Ultra5 field emission scanning electron microscope, transmission electron microscopy with an FEI Tecnai F20 twin transmission electron microscope, X-Ray diffraction on a Rigaku Ultima III X-ray diffractometer, and optical microscopy using a Keyence VHX 6000 digital microscope. The optical spectra were acquired with an Ideaoptics PG2000-Pro fiber optical spectrometer equipped with a 50 mm integrating sphere. The thickness of the filtered film was determined by the optical height profile acquired from the digital microscope. In order to evaluate the electrical properties, the deformable liquid metal contacts were printed onto the samples through paper stencils. The resistance was measured under a four-probe configuration by using a Keithley 2110 multimeter. The mechanical strains were applied by homemade motorized linear stages under uniaxial, biaxial, and twisting configurations.

Electrochemical and Mechanical Measurement: The electrochemical measurements were primarily performed by using a CHI660E electrochemical workstation. EIS was conducted in the frequency range from 0.1 Hz to 100 kHz with an amplitude of 10 mV at the open circuit potential. Galvanostatic cyclic performance was studied by using a Land CT3001A battery testing system. The active area was calculated considering the area of interdigital electrodes and their interspaces.

Supporting Information

Supporting Information is available from the Wiley Online Library or from the author.

Acknowledgements

The authors acknowledge the support from the National Key Research and Development Program of China (grant no. 2022YFA1405000), the Natural Science Foundation of Jiangsu Province, Major Project (grant no. BK20212004), the Key Research and Development Program of Jiangsu Provincial Department of Science and Technology of China (grant no. BE2019002), the China Postdoctoral Science Foundation (grant no. 2020M681549), and the Postgraduate Research & Practice Innovation Program of Jiangsu Province.

Conflict of Interest

The authors declare no conflict of interest.

Data Availability Statement

The data that support the findings of this study are available in the supplementary material of this article.

Keywords

microsupercapacitors, MXene, stretchable electronics, stretchable energy storage devices, wearable electronics

Received: January 13, 2023

Published online: February 23, 2023

- [1] Z. Ma, D. Kong, L. Pan, Z. Bao, *J. Semicond.* **2020**, *41*, 041601.
- [2] D. C. Kim, H. J. Shim, W. Lee, J. H. Koo, D. H. Kim, *Adv. Mater.* **2020**, *32*, 1902743.
- [3] J. A. Rogers, T. Someya, Y. G. Huang, *Science* **2010**, *327*, 1603.
- [4] S. Wang, J. Y. Oh, J. Xu, H. Tran, Z. Bao, *Acc. Chem. Res.* **2018**, *51*, 1033.
- [5] S. Wang, J. Xu, W. Wang, G. N. Wang, R. Rastak, F. Molina-Lopez, J. W. Chung, S. Niu, V. R. Feig, J. Lopez, T. Lei, S. K. Kwon, Y. Kim, A. M. Foudeh, A. Ehrlich, A. Gasperini, Y. Yun, B. Murmann, J. B. Tok, Z. Bao, *Nature* **2018**, *555*, 83.
- [6] H. U. Chung, B. H. Kim, J. Y. Lee, J. Lee, Z. Xie, E. M. Ibler, K. Lee, A. Banks, J. Y. Jeong, J. Kim, C. Ogle, D. Grande, Y. Yu, H. Jang, P. Assem, D. Ryu, J. W. Kwak, M. Namkoong, J. B. Park, Y. Lee, D. H. Kim, A. Ryu, J. Jeong, K. You, B. Ji, Z. Liu, Q. Huo, X. Feng, Y. Deng, et al., *Science* **2019**, *363*, 947.
- [7] J. Kim, A. S. Campbell, B. E. de Avila, J. Wang, *Nat. Biotechnol.* **2019**, *37*, 389.
- [8] D. Son, J. Lee, S. Qiao, R. Ghaffari, J. Kim, J. E. Lee, C. Song, S. J. Kim, D. J. Lee, S. W. Jun, S. Yang, M. Park, J. Shin, K. Do, M. Lee, K. Kang, C. S. Hwang, N. Lu, T. Hyeon, D. H. Kim, *Nat. Nanotechnol.* **2014**, *9*, 397.
- [9] X. M. G. Yao, C. Yin, W. Lou, Q. Wang, S. Huang, L. Mao, S. Chen, K. Zhao, T. Pan, *Sci. Adv.* **2022**, *9*, eabl8379.
- [10] J. W. Jeong, W. H. Yeo, A. Akhtar, J. J. Norton, Y. J. Kwack, S. Li, S. Y. Jung, Y. Su, W. Lee, J. Xia, H. Cheng, Y. Huang, W. S. Choi, T. Bretl, J. A. Rogers, *Adv. Mater.* **2013**, *25*, 6839.
- [11] H. Zhao, Y. Zhou, S. Cao, Y. Wang, J. Zhang, S. Feng, J. Wang, D. Li, D. Kong, *ACS Mater. Lett.* **2021**, *3*, 912.
- [12] M. Wang, Z. Yan, T. Wang, P. Cai, S. Gao, Y. Zeng, C. Wan, H. Wang, L. Pan, J. Yu, S. Pan, K. He, J. Lu, X. Chen, *Nat. Electron.* **2020**, *3*, 563.
- [13] Y. Wang, Y. Ding, X. Guo, G. Yu, *Nano Res.* **2019**, *12*, 1978.
- [14] D. J. Lipomi, Z. Bao, *Energy Environ.* **2011**, *4*, 3314.
- [15] K. Keum, J. W. Kim, S. Y. Hong, J. G. Son, S. S. Lee, J. S. Ha, *Adv. Mater.* **2020**, *32*, 2002180.
- [16] W. Liu, M. S. Song, B. Kong, Y. Cui, *Adv. Mater.* **2017**, *29*, 1603436.
- [17] X. Gong, Q. Yang, C. Zhi, P. S. Lee, *Adv. Energy Mater.* **2020**, *11*, 2003308.
- [18] D. G. Mackanic, T. H. Chang, Z. Huang, Y. Cui, Z. Bao, *Chem. Soc. Rev.* **2020**, *49*, 4466.
- [19] G. Chen, Y. Li, M. Bick, J. Chen, *Chem. Rev.* **2020**, *120*, 3668.
- [20] X. Li, H. Li, X. Fan, X. Shi, J. Liang, *Adv. Energy Mater.* **2020**, *10*, 1903794.
- [21] S. Y. Hong, J. Yoon, S. W. Jin, Y. Lim, S. J. Lee, G. Zi, J. S. Ha, *ACS Nano* **2014**, *8*, 8844.
- [22] J. Pu, X. Wang, R. Xu, K. Komvopoulos, *ACS Nano* **2016**, *10*, 9306.
- [23] M. Beidaghi, Y. Gogotsi, *Energy Environ.* **2014**, *7*, 867.
- [24] N. A. Kyeremateng, T. Brousse, D. Pech, *Nat. Nanotechnol.* **2017**, *12*, 7.
- [25] Z.-S. Wu, X. Feng, H.-M. Cheng, *Natl. Sci. Rev.* **2014**, *1*, 277.
- [26] D. Kim, G. Shin, Y. J. Kang, W. Kim, J. S. Ha, *ACS Nano* **2013**, *7*, 7975.
- [27] G. Lee, D. Kim, D. Kim, S. Oh, J. Yun, J. Kim, S.-S. Lee, J. S. Ha, *Energy Environ.* **2015**, *8*, 1764.
- [28] Z. Niu, H. Dong, B. Zhu, J. Li, H. H. Hng, W. Zhou, X. Chen, S. Xie, *Adv. Mater.* **2013**, *25*, 1058.
- [29] D. Qi, Z. Liu, Y. Liu, W. R. Leow, B. Zhu, H. Yang, J. Yu, W. Wang, H. Wang, S. Yin, X. Chen, *Adv. Mater.* **2015**, *27*, 5559.
- [30] J. Yun, H. Lee, C. Song, Y. R. Jeong, J. W. Park, J. H. Lee, D. S. Kim, K. Keum, M. S. Kim, S. W. Jin, Y. H. Lee, J. W. Kim, G. Zi, J. S. Ha, *Chem. Eng. J.* **2020**, *387*, 124076.
- [31] G. Lee, J. W. Kim, H. Park, J. Y. Lee, H. Lee, C. Song, S. W. Jin, K. Keum, C. H. Lee, J. S. Ha, *ACS Nano* **2019**, *13*, 855.
- [32] T. H. Chang, T. Zhang, H. Yang, K. Li, Y. Tian, J. Y. Lee, P. Y. Chen, *ACS Nano* **2018**, *12*, 8048.
- [33] F. Tehrani, M. Beltrán-Gastélum, K. Sheth, A. Karajic, L. Yin, R. Kumar, F. Soto, J. Kim, J. Wang, S. Barton, M. Mueller, J. Wang, *Adv. Mater. Technol.* **2019**, *4*, 1900162.
- [34] L. Li, Z. Lou, W. Han, D. Chen, K. Jiang, G. Shen, *Adv. Mater. Technol.* **2017**, *2*, 1600282.
- [35] A. V. Mohammadi, J. Rosen, Y. Gogotsi, *Science* **2021**, *372*, 1165.
- [36] B. Anasori, M. R. Lukatskaya, Y. Gogotsi, *Nat. Rev. Mater.* **2017**, *2*, 16098.
- [37] X. Li, Z. Huang, C. E. Shuck, G. Liang, Y. Gogotsi, C. Zhi, *Nat. Rev. Chem.* **2022**, *6*, 389.
- [38] M. R. Lukatskaya, S. Kota, Z. Lin, M.-Q. Zhao, N. Shpigel, M. D. Levi, J. Halim, P.-L. Taberna, M. W. Barsoum, P. Simon, Y. Gogotsi, *Nat. Energy* **2017**, *2*, 17105.
- [39] J. Pang, R. G. Mendes, A. Bachmatiuk, L. Zhao, H. Q. Ta, T. Gemming, H. Liu, Z. Liu, M. H. Rummeli, *Chem. Soc. Rev.* **2019**, *48*, 72.
- [40] M. Q. Zhao, C. E. Ren, Z. Ling, M. R. Lukatskaya, C. Zhang, K. L. Van Aken, M. W. Barsoum, Y. Gogotsi, *Adv. Mater.* **2015**, *27*, 339.
- [41] R. B. Rakhi, B. Ahmed, M. N. Hedhili, D. H. Anjum, H. N. Alshareef, *Chem. Mater.* **2015**, *27*, 5314.
- [42] S. Feng, X. Wang, M. Wang, C. Bai, S. Cao, D. Kong, *Nano Lett.* **2021**, *21*, 7561.
- [43] Y. Zhou, K. Maleski, B. Anasori, J. O. Thostenson, Y. Pang, Y. Feng, K. Zeng, C. B. Parker, S. Zauscher, Y. Gogotsi, J. T. Glass, C. Cao, *ACS Nano* **2020**, *14*, 3576.
- [44] H. Hu, Z. Bai, B. Niu, M. Wu, T. Hua, *J. Mater. Chem. A* **2018**, *6*, 14876.
- [45] S. Jiao, A. Zhou, M. Wu, H. Hu, *Adv. Sci.* **2019**, *6*, 1900529.
- [46] P. L. Floch, S. Meixuanzi, J. Tang, J. Liu, Z. Suo, *ACS Appl. Mater. Interfaces* **2018**, *10*, 27333.

- [47] X. Chen, S. Wang, J. Shi, X. Du, Q. Cheng, R. Xue, Q. Wang, M. Wang, L. Ruan, W. Zeng, *Adv. Mater. Interfaces* **2019**, 6, 1901160.
- [48] Q. Li, Q. Wang, L. Li, L. Yang, Y. Wang, X. Wang, H. T. Fang, *Adv. Energy Mater.* **2020**, 10, 2000470.
- [49] Y. Xuan, X. Guo, Y. Cui, C. Yuan, H. Ge, B. Cui, Y. Chen, *Soft Matter* **2012**, 8, 9603.
- [50] C. Cho, P. Kang, A. Taqieddin, Y. Jing, K. Yong, J. M. Kim, M. F. Haque, N. R. Aluru, S. Nam, *Nat. Electron.* **2021**, 4, 126.
- [51] P. Görrn, W. Cao, S. Wagner, *Soft Matter* **2011**, 7, 7177.
- [52] S. Abdolhosseinzadeh, R. Schneider, A. Verma, J. Heier, F. Nuesch, C. J. Zhang, *Adv. Mater.* **2020**, 32, 2000716.
- [53] Z. Zhao, S. Wang, F. Wan, Z. Tie, Z. Niu, *Adv. Funct. Mater.* **2021**, 31, 2101302.
- [54] S. Yu, Y. Sun, Y. Ni, X. Zhang, H. Zhou, *ACS Appl. Mater. Interfaces* **2016**, 8, 5706.
- [55] H. Huang, H. Su, H. Zhang, L. Xu, X. Chu, C. Hu, H. Liu, N. Chen, F. Liu, W. Deng, B. Gu, H. Zhang, W. Yang, *Adv. Electron. Mater.* **2018**, 4, 1800179.
- [56] D. Tu, W. Yang, Y. Li, Y. Zhou, L. Shi, J. Xu, Y. Yang, *J. Mater. Chem. C* **2021**, 9, 11104.
- [57] L. Qin, Q. Tao, X. Liu, M. Fahlman, J. Halim, P. O. Å. Persson, J. Rosen, F. Zhang, *Nano Energy* **2019**, 60, 734.
- [58] C. J. Zhang, M. P. Kremer, A. Seral-Ascaso, S.-H. Park, N. McEvoy, B. Anasori, Y. Gogotsi, V. Nicolosi, *Adv. Funct.* **2018**, 31, 1705506.
- [59] Y. Yue, N. Liu, Y. Ma, S. Wang, W. Liu, C. Luo, H. Zhang, F. Cheng, J. Rao, X. Hu, J. Su, Y. Gao, *ACS Nano* **2018**, 12, 4224.
- [60] Y.-Y. Peng, B. Akuzum, N. Kurra, M.-Q. Zhao, M. Alhabeb, B. Anasori, E. C. Kumbur, H. N. Alshareef, M.-D. Ger, Y. Gogotsi, *Energy Environ. Sci.* **2016**, 9, 2847.
- [61] S. Li, T.-H. Chang, Y. Li, M. Ding, J. Yang, P.-Y. Chen, *J. Mater. Chem. A* **2021**, 9, 4664.